JCTC Journal of Chemical Theory and Computation

Article

pubs.acs.org/JCTC

Tensor Hypercontraction Second-Order Møller–Plesset Perturbation Theory: Grid Optimization and Reaction Energies

Sara I. L. Kokkila Schumacher,[†,‡] Edward G. Hohenstein,[†,‡,§] Robert M. Parrish,[∥] Lee-Ping Wang,[†,‡] and Todd J. Martínez*[,†,‡]

[†]Department of Chemistry and the PULSE Institute, Stanford University, Stanford, California 94305, United States

[‡]SLAC National Accelerator Laboratory, Menlo Park, California 94025, United States

[§]Department of Chemistry and Biochemistry, City College of New York, New York, New York 10031, United States

[∥]Center for Computational Molecular Science and Technology, School of Chemistry and Biochemistry, Georgia Institute of Technology, Atlanta, Georgia 30332-0400, United States

Supporting Information

ABSTRACT: We have recently introduced the tensor hypercontraction (THC) method for electronic structure, including MP2. Here, we present an algorithm for THC-MP2 that lowers the memory requirements as well as the prefactor while maintaining the formal quartic scaling that we demonstrated previously. We also describe a procedure to optimize quadrature grids used in grid-based least-squares (LS) THC-MP2. We apply this algorithm to generate grids for first-row atoms with less than 100 points/atom while incurring negligible errors in the computed energies. We benchmark the LS-THC-MP2 method using optimized grids for a wide variety of tests sets including conformational energies and reaction barriers in both the cc-pVDZ and cc-pVTZ basis sets. These tests demonstrate that the THC methodology is not limited to small basis sets and that it incurs negligible errors in both absolute and relative energies.

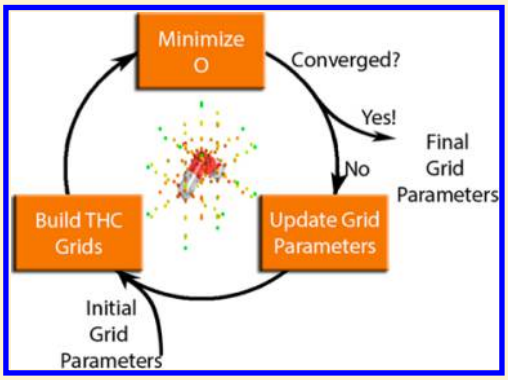

I. INTRODUCTION

Second-order Møller–Plesset perturbation theory (MP2) is the simplest post-HF method for including electron correlation.[1] It strikes a practical balance between accuracy and efficiency that makes it applicable to many systems of chemical interest. However, canonical MP2 scales as $O(N^5)$, where N is the number of basis functions and is proportional to molecular size. This steep scaling limits its practical use to small molecules. This scaling is due to the transformation of the electron repulsion integrals (ERIs) from the atomic orbital (AO) basis to the molecular orbital (MO) basis.

A number of different approaches have been applied in an effort to decrease the computational cost of MP2. Atomic orbital formulations allow exploitation of the sparsity of ERIs in the AO basis.[2−6] Factorization of the orbital energy denominator via the Laplace transformation or a Cholesky decomposition (CD) is often combined with the AO basis formulations, including recent work by Ochsenfeld and co-workers.[5,7,8] In other formulations, the ERIs are represented in terms of localized orthogonal orbitals. Local correlation methods allow one to neglect pair correlation between distant localized orbitals.[9−12] This approximation can be combined with other techniques to reduce the cost.[13] Other localized orbital techniques, such as the pair natural orbital (PNO) approach and the orbital-specific virtuals (OSVs) approach, have been used to reduce the prefactor in local MP2 and other methods.[14−21] Both AO formulations and local correlation methods in combination with other techniques have led to linear-scaling MP2 methods.[22−24] Unfortunately, reducing the overhead computational cost associated with different linear-scaling approaches is still a key challenge.[25,26] Furthermore, there has been progress in mitigating the difficulties with discontinuities in potential energy surfaces, but *ab initio* molecular dynamics with these approaches is not straightforward.[27,28]

Other methods involve the decomposition of the ERI into more computationally efficient forms. There are at least three methods for ERI decomposition that have been previously applied to MP2. In each case, there are auxiliary indices (whose range scales linearly with molecular size) that we label uniformly as P and Q to highlight the similarities in the methods. In the pseudospectral method, the ERIs are partially evaluated numerically and partially evaluated analytically through the use of transformations between spectral and physical space.[29−34] This leads to a formulation of the ERI as a product of a third-order tensor and two matrices

$$(\mu\nu|\lambda\sigma) \approx \sum_{P} Q_{\mu P}\bar{R}_{P\nu}A_{P,\lambda\sigma} \tag{1}$$

Received: March 23, 2015
Published: June 12, 2015

DOI: 10.1021/acs.jctc.5b00272
J. Chem. Theory Comput. 2015, 11, 3042−3052

where

$$\mathbf{Q} = \mathbf{S}[\bar{\mathbf{R}}^t\mathbf{w}\bar{\mathbf{R}}]^{-1}\bar{\mathbf{R}}^t\mathbf{w} \tag{2}$$

and

$$A_{P,\lambda\sigma} = \int \frac{\phi_\lambda(\vec{r})\,\phi_\sigma(\vec{r})}{|\vec{r}_P - \vec{r}|}\,\mathrm{d}\vec{r} \tag{3}$$

Here, $\bar{\mathbf{R}}$ is a collocation matrix, the diagonal matrix $\mathbf{w}$ contains the grid point weights, grid points indexed by P are located at $\vec{r}_p$, and $\mathbf{S}$ is the overlap matrix for the basis functions ϕ_μ. A similar factorization can be achieved by using a pivoted incomplete Cholesky decomposition of the ERI matrix.[35−38] This allows the ERI tensor to be written in the form

$$(\mu\nu|\lambda\sigma) \approx \sum_P L_{\mu\nu,P}L_{\lambda\sigma,P} \tag{4}$$

The density fitting (DF) approach, also known as the resolution of the identity (RI), leads to a similar factorization through a somewhat different route.[7,39−44] Instead of a Cholesky decomposition of the integral matrix, the DF technique fits generalized densities using an auxiliary basis set (χ_P)

$$\phi_\mu(\vec{r})\,\phi_\nu(\vec{r}) \approx \sum_P d_{\mu\nu,P}\chi_P(\vec{r}) \tag{5}$$

where $d_{\mu\nu,P}$ are density fitting coefficients. Several different fitting metrics have been developed to determine the density fitting coefficients.[45−48] Auxiliary basis sets have been optimized[49,50] within the commonly used Coulomb fitting metric, often referred to as DF(J). Other ERI factorization techniques, such as decomposing the two-electron integrals into a representation with the canonical product tensor format, have been applied to MP2 and coupled cluster theory to reduce storage requirements or computational effort.[51,52]

Each of these ERI factorization techniques has been able to provide some computational relief in MP2 while also maintaining chemical accuracy in the computation of energy differences.[33,41,53−55] However, there are also distinct weaknesses that need to be addressed. We first illustrate the primary weakness of DF approaches using the construction of the Fock matrix as an example. In DF, the Coulomb contributions can be expressed in terms of the two- and three-center integrals

$$(J_{\mathrm{DF}})_{PQ} \equiv (P|Q) = \int \chi_P(\vec{r}_1)\frac{1}{r_{12}}\chi_Q(\vec{r}_2)\,d\vec{r}_1\,d\vec{r}_2 \tag{6}$$

and

$$(\mu\nu|P) = \int \phi_\mu(\vec{r}_1)\,\phi_\nu(\vec{r}_1)\frac{1}{r_{12}}\chi_P(\vec{r}_2)\,d\vec{r}_1\,d\vec{r}_2 \tag{7}$$

and the Coulomb contribution to the Fock matrix is expressed as

$$J_{\mu\nu} \approx \sum_{PQ\lambda\sigma} (\mu\nu|P)(J^{-1}_{\mathrm{DF}})_{PQ}(Q|\lambda\sigma)D_{\lambda\sigma} \tag{8}$$

where $D_{\lambda\sigma}$ represents the density matrix. Defining

$$c^P = \sum_{\lambda\sigma} (P|\lambda\sigma)D_{\lambda\sigma} \tag{9}$$

$$d^P = \sum_Q (J^{-1}_{\mathrm{DF}})_{PQ}c^Q \tag{10}$$

Equation 8 can be expressed as

$$J_{\mu\nu} = \sum_P (\mu\nu|P)d^P \tag{11}$$

In this formulation, the Coulomb contribution scales as $O(N^3)$, where we use the fact that the range of the auxiliary index is linear in the molecular size. In contrast, DF is unable to produce any scaling advantage for the exchange contribution, which can be represented as

$$K_{\mu\nu} = \sum_{PQ\lambda\sigma} (\mu\lambda|P)(J^{-1}_{\mathrm{DF}})_{PQ}(Q|\nu\sigma)D_{\lambda\sigma} \tag{12}$$

This can be evaluated as

$$c^Q_{\nu\lambda} = \sum_\sigma (Q|\nu\sigma)D_{\lambda\sigma} \tag{13}$$

$$d^P_{\nu\lambda} = \sum_Q (J^{-1}_{\mathrm{DF}})_{PQ}c^Q_{\nu\lambda} \tag{14}$$

$$K_{\mu\nu} = \sum_{P\lambda} (\mu\lambda|P)d^P_{\nu\lambda} \tag{15}$$

which scales as $O(N^4)$. There is thus no scaling reduction in the computation of exchange with DF, and the problem lies in the "pinning" of the μ and ν indices. Note that for exchange matrices in SCF the low-rank factorization of the one particle density matrix (D) into the product of occupied orbital coefficients can be used to reduce the prefactor but not the scaling.[56] This inability to factor exchange-like terms manifests in DF-MP2 as well, where it prevents the $O(N^5)$ scaling of MP2 from being reduced. Because CD approaches maintain the pinning of the μ and ν indices, these suffer from the same problem. Pseudospectral methods are able to reduce the scaling of exchange terms, because the μ and ν indices are unpinned (although the λ and σ indices remain pinned). However, this comes with a difficulty in maintaining the permutational symmetry of the integrals, and this can have a deleterious effect on accuracy and stability.

Recently, an alternative ERI factorization method known as tensor hypercontraction (THC) was introduced.[57] This technique is the first to efficiently allow full separation of all four indices in the ERI. In general, the THC factorization of the ERI tensor is represented as

$$(\mu\nu|\lambda\sigma) \approx \sum_{PQ} X^P_\mu X^P_\nu Z^{PQ} X^Q_\lambda X^Q_\sigma \tag{16}$$

In this notation, X and Z are matrices, whereas P and Q denote auxiliary indices. Within the THC representation, all four of the ERI indices are effectively completely unpinned. This additional flexibility allows factorization of exchange-like terms. In particular, it allows the scaling of MP2 to be reduced from $O(N^5)$ to $O(N^4)$, regardless of whether the method is formulated in the atomic or molecular orbital basis. Furthermore, the index permutation symmetry of the integrals is guaranteed by construction, as long as the matrix Z is symmetric.

There are a number of possible ways to achieve the integral factorization in eq 16. In this work, we use the least-squares approach (LS-THC),[58] which asserts a form for the X matrices and solves for the optimal Z matrix by least-squares fitting to minimize the error in the integrals (specifically, the 2-norm of the difference between the exact and factorized integrals). In

DOI: 10.1021/acs.jctc.5b00272
J. Chem. Theory Comput. 2015, 11, 3042−3052

grid-based LS-THC, the X matrices are chosen to be collocation matrices for a physical space grid, i.e.

$$X_\mu^P = \sqrt[4]{w_P}\,\phi_\mu(\vec{r}_P) \tag{17}$$

where w_P is a weighting factor associated with the Pth grid point (located at r_P). This grid-based LS-THC approach to MP2 has been demonstrated to be very accurate (errors compared to DF-MP2 of less than 0.1 kcal/mol) for a number of test molecules containing up to ≈60 atoms.[58] However, the physical space grids used to form the X factors were not optimized for use with LS-THC-MP2. In this work, we present an optimization scheme to tailor grids for use with LS-THC-MP2 and show that a more than 2-fold reduction in the number of grid points can be achieved. We apply this approach to optimize grids for both the cc-pVDZ and cc-pVTZ basis sets, showing that the LS-THC approach is not restricted to small basis sets. Previous assessments of the errors associated with the THC factorization have focused on absolute energies at specific geometries. It is also important to ensure that any THC errors are weakly varying with molecular geometry. In this work, we investigate the behavior of errors in reaction energies and barrier heights in order to demonstrate that the THC error (using the optimized grids presented here) is negligible for chemical purposes. Several benchmark sets have been chosen to represent conformational effects, hydrogen-bonding configurations, and reaction barrier heights. The molecules in these sets range in size from 9 to over 450 atoms.

II. NOTATION

We use the Greek letters μ, ν, λ, and σ to denote one of the N atomic orbital (AO) basis functions. In this work, these are atom-centered contracted Gaussian functions. The particular form of LS-THC that we use here relies on an intermediate DF approximation. The associated DF auxiliary basis indices (of which there are N_{aux} members) will be represented by A and B. The letters P, Q, R, and S are used to indicate one of the N_P auxiliary indices or grid point indices for the THC two-electron integrals. The letters i and j represent one of the N_O occupied MO basis functions, whereas the letters a and b represent one of the N_V virtual MOs. Finally, we also use a Laplace transformation to treat the orbital energy denominators. The Laplace-transformed denominators are denoted τ_i^ν, where i denotes the MO and ν indexes the Laplace quadrature points.

III. THEORY

III.A. LS-THC Integrals. In the grid-based formulation of LS-THC, the X factors are given as collocation matrices, as defined in eq 17. The matrix Z^{PQ} is then obtained by minimizing the square of the 2-norm of the residual. In other words, we define the error as

$$\Delta \equiv \frac{1}{2}\left|\left|(\mu\nu|\lambda\sigma) - \sum_{PQ} R_{\mu\nu}^P Z^{PQ} R_{\lambda\sigma}^Q\right|\right|_2^2 \tag{18}$$

where the joint collocation matrix is defined as $R_{\mu\nu}^P = X_\mu^P X_\nu^P$. Minimizing the error with respect to the elements of Z^{PQ}, and defining the physical space overlap matrix $\mathbf{S}_{\text{phys}}$ as

$$(S_{\text{phys}})_{PQ} = \sum_{\mu\nu} R_{\mu\nu}^P R_{\mu\nu}^Q \tag{19}$$

we arrive at an analytical solution

$$Z^{PQ} = (\mathbf{S}_{\text{phys}}^{-1}\mathbf{V}^{\text{phys}}\mathbf{S}_{\text{phys}}^{-1})_{PQ} \tag{20}$$

where we use the fact that $\mathbf{S}_{\text{phys}}$ is real symmetric and $\mathbf{V}^{\text{phys}}$ is a physical space projection of the ERIs

$$V_{PQ}^{\text{phys}} = \sum_{\mu\nu\lambda\sigma} R_{\mu\nu}^P (\mu\nu|\lambda\sigma) R_{\lambda\sigma}^Q \tag{21}$$

If the fully analytic ERIs are used to construct $\mathbf{V}^{\text{phys}}$, then the formation of Z^{PQ} will scale as $O(N^5)$ due to eq 21. This effort for the formation of Z^{PQ} can be reduced to $O(N^4)$ by introducing a DF approximation for the ERIs (in the Coulomb metric here, but other metrics could also be used)[7]

$$V_{PQ}^{\text{phys,DF}} = \sum_{\mu\nu\lambda\sigma AB} R_{\mu\nu}^P (\mu\nu|A)(J_{\text{DF}}^{-1})_{AB}(B|\lambda\sigma) R_{\lambda\sigma}^Q \tag{22}$$

This sequence of approximations is known as grid-based LS-THC-DF-MP2. It is important to emphasize that N_P must be less than N^2 for the procedure to be computationally advantageous. When N_P is greater or equal to N^2, the least-squares formulation of eq 20 is formally exact (as long as there are no linear dependencies). In this case, there is also no computational gain, as can be seen below. However, we find that the number of grid points needed to achieve accurate results is far less than N^2 and, in fact, scales linearly with N. This makes the factorization highly advantageous, leading to scaling reductions of up to 2 powers of the molecular size so far.[57−62]

III.B. THC-MP2. Using the LS-THC-DF-MP2 representation, an alternative factorization of THC-MP2 has been implemented. In order to effectively factorize the MP2 energy expression, we first must deal with the orbital energy denominators

$$\Lambda_{ij}^{ab} = \frac{1}{\varepsilon_a + \varepsilon_b - \varepsilon_i - \varepsilon_j} \tag{23}$$

We exploit the Laplace transformation[63] and a subsequent numerical quadrature[51]

$$\Lambda_{ij}^{ab} = \int_0^\infty e^{-(\varepsilon_a+\varepsilon_b-\varepsilon_i-\varepsilon_j)t}\,dt \approx \sum_\nu \tau_a^\nu \tau_b^\nu \tau_i^\nu \tau_j^\nu \tag{24}$$

By combining the THC approximation and the Laplace transformation, the MP2 energy expression can be written as

$$E_{\text{MP2}} \approx -\sum_{abij\nu PQRS} \tau_a^\nu \tau_b^\nu \tau_i^\nu \tau_j^\nu X_i^P X_a^P Z^{PQ} X_j^Q X_b^Q \times (2X_i^R X_a^R Z^{RS} X_j^S X_b^S - X_i^R X_b^R Z^{RS} X_j^S X_a^S) \tag{25}$$

With construction of the appropriate intermediates, this can be evaluated in $O(N^4)$ operations. However, there are many different ways to achieve this. Our previous implementation[57] of THC-MP2 proved that quartic scaling was achievable, but it did not focus on the prefactor. Here, we concentrate on reducing the prefactor while maintaining quartic scaling. The Coulomb-like contributions to the MP2 correlation energy, described in Scheme 1, are formed in the same way as that outlined previously. This part of the calculation scales only as $O(N^3)$ and thus is usually not a bottleneck if exchange contributions are also included.

Scheme 2 presents an alternative factorization for the exchange-like contributions to the MP2 correlation energy (involving the second term in parentheses in eq 25). After obtaining the Coulomb-like energy contributions, we block

DOI: 10.1021/acs.jctc.5b00272
J. Chem. Theory Comput. 2015, 11, 3042−3052

Scheme 1. Pseudocode for the Coulomb-like Contributions to the LS-THC-DF-MP2 Energy

For each Laplace quadrature point ν

$$O^{PR\nu} = \sum_i \tau_i^\nu X_i^P X_i^R \qquad O(N_P^2 N_O)$$

$$V^{PR\nu} = \sum_a \tau_a^\nu X_a^P X_a^R \qquad O(N_P^2 N_V)$$

$$A^{PR\nu} = O^{PR\nu} V^{PR\nu} \qquad O(N_P^2)$$

$$B^{QR\nu} = \sum_P A^{PR\nu} Z^{PQ} \qquad O(N_P^3)$$

$$E_{MP2-J} += \sum_{QR} -2 B^{QR\nu} B^{RQ\nu} \qquad O(N_P^2)$$

end for

Scheme 2. Pseudocode for the Exchange-like Contributions to the LS-THC-DF-MP2 Energy[a]

For each i_{block}

$$A_{ia}^P = X_i^P X_a^P \qquad O(N_P N_O N_V)$$

$$B_{ia}^Q = \sum_P A_{ia}^P Z^{PQ} \qquad O(N_P^2 N_O N_V)$$

For each Laplace quadrature point ν

$$C_{ia}^{Q\nu} = \tau_a^\nu B_{ia}^Q \qquad O(N_P N_O N_V)$$

$$D_i^{QS\nu} = \sqrt{\tau_i^\nu} \sum_a X_a^S C_{ia}^{Q\nu} \qquad O(N_P^2 N_O N_V)$$

$$E^{QS\nu} = \sum_{i \in i_{block}} D_i^{QS\nu} D_i^{SQ\nu} \qquad O(N_P^2 N_O)$$

$$F^{QS\nu} = \sum_j \tau_j^\nu X_j^Q X_j^S \qquad O(N_P^2 N_O)$$

$$E_{MP2-K} += \sum_{QS} E^{QS\nu} F^{QS\nu} \qquad O(N_P^2)$$

end for

end for

[a]The size of i_{block} is determined by the amount of memory available.

over the occupied index, i, carrying out the exchange factorization for each i_{block}. This algorithm for the exchange-like energy contributions is formulated to carry the occupied, i, index through as many intermediates as possible. This has a minimum memory requirement of $O(N^2)$ as opposed to the $O(N^3)$ memory requirement to store the full three index quantities. The exchange-like algorithm described in this work has reduced memory requirements and a reduced prefactor relative to those of the previously published LS-THC-DF-MP2 algorithm for the exchange contributions. With a formal scaling of $O(N^4)$, LS-THC-DF-MP2 is a lower scaling alternative to conventional MP2 as well as DF-MP2.

III.C. Grid Optimization. In the LS-THC grid based method, the X factors are defined by a physical space quadrature with N_P grid points. We construct the grids following the usual procedure for numerical integration as used in density functional theory. The full molecular quadrature grid is constructed from atom-centered spherical quadratures. To form the atom-centered spherical quadratures, a direct product of angular $\{\langle \Omega_Q, w_Q^\Omega \rangle\}$ and radial $\{\langle \rho_Q, w_Q^\rho \rangle\}$ coordinates (and their corresponding weights) is used, i.e.[64]

$$\{\langle \vec{r}_Q, w_Q \rangle\} \equiv \{\langle \rho_Q, w_Q^\rho \rangle \otimes \langle \Omega_Q, w_Q^\Omega \rangle\} \tag{26}$$

For the spherical coordinate, the natural choice of quadrature rule is the family of Lebedev–Laikov grids.[65] In our previous work, we used either the predetermined Treutler–Ahlrichs quadrature from DFT grids or a technique known as radial discrete variable representation (R-DVR) to provide the radial quadrature rules.[66] In this work, we treat the radial quadrature as an adjustable set of parameters, which we will optimize and tabulate for specific basis sets, much as is done for DF auxiliary basis sets. For reasons to be made clear shortly, we denote this class of THC grids as Handy grids. In this approach, the radial nodes, ρ_Q in $[0,\infty)$, will be the only free parameter in the optimization procedure outlined below. To provide an automatic set of radial weights, w_Q^ρ, for a given set of radial nodes, an irregularly spaced variant of the trapezoid rule, motivated by the Handy radial scheme in DFT, is applied.[67,68] First, a mapping of the radial nodes from $[0,\infty)$ to $[0,1]$ is defined

$$x_Q = \frac{1}{1 + \sqrt{R/\rho_Q}} \tag{27}$$

where R is the Bragg–Slater radius of the atom. The radial weights are then given as

$$w_Q^\rho = [x_{Q+1} - x_{Q-1}] \frac{x_Q^5 R^3}{(1 - x_Q)^7} \tag{28}$$

where $x_0 \equiv 0$ and $x_{N_\rho+1} \equiv 1$ for radial grid point indices $Q \in [1,N_\rho]$.

Once an atomic grid is built for each atom, the rules of Gill et al. are used to rotate the atomic grids into a standard molecular orientation.[69,70] The final molecular grid is formed from the weighted sum of the atomic quadrature grids, with the Treutler–Ahlrichs version of Becke's fuzzy Voronoi partition used to form the atomic weights.[66] A more detailed description of the molecular grid formation is included in Sections I and II.A of the Supporting Information.

In order to optimize the radial quadrature grids, we modified an approach previously used to optimize auxiliary basis sets in DF-MP2.[49] This approach chose auxiliary basis functions to minimize the objective function

$$\Delta = -\frac{1}{4} \sum_{iajb} \frac{|\langle ij||ab\rangle_{\text{exact}} - \langle ij||ab\rangle_{\text{approx}}|^2}{\varepsilon_i + \varepsilon_j - \varepsilon_a - \varepsilon_b} \tag{29}$$

evaluated over a set of small molecules, where the double bar denotes an antisymmetrized two-electron integral. We adopt a similar approach to optimize the Handy grids tailored specifically to represent the ERIs in LS-THC-DF-MP2. We avoid optimizing the Handy grids with molecules where the number of grid points is high relative to the basis set size, since the THC integral approximation reproduces the DF integrals exactly when the number of grid points is large. Accordingly, the molecules in our training set (see Supporting Information Table S1) are significantly larger than those used to optimize auxiliary basis sets for DF-MP2. The optimization begins with an initial guess from a trimmed R-DVR grid that has approximately half the number of radial points as the R-DVR grid previously used in THC.[64]

DOI: 10.1021/acs.jctc.5b00272
J. Chem. Theory Comput. 2015, 11, 3042–3052

In order to succinctly define the objective function, we will denote the differences between the density fitted integrals and the LS-THC integrals as

$$\Delta_{ij}^{ab} = (ia|jb)_{\mathrm{DF}} - (ia|jb)_{\mathrm{THC}} \tag{30}$$

Recall from eqs 16 and 17

$$\begin{aligned}(ia|jb)_{\mathrm{THC}} &= \sum_{PQ} X_i^P X_a^P Z^{PQ} X_j^Q X_b^Q \\ &= \sum_{PQ} \sqrt{w_P w_Q}\, \phi_i(\vec{r}_P)\, \phi_a(\vec{r}_P)\, Z^{PQ} \phi_j(\vec{r}_Q)\, \phi_b(\vec{r}_Q)\end{aligned} \tag{31}$$

which clarifies the dependence of the THC integrals on the placement of the angular and radial coordinates of the quadrature points. We define the objective function to be minimized as

$$O = \sum_{m \in \text{test set}} \frac{1}{E_m^{\mathrm{MP2}}} \sum_{iajb} \frac{(\Delta_{ij}^{ab}(m))^2 + \frac{1}{2}(\Delta_{ij}^{ab}(m) - \Delta_{ij}^{ba}(m))^2}{\varepsilon_a + \varepsilon_b - \varepsilon_i - \varepsilon_j} \tag{32}$$

where m labels the molecules in the test set and E_m^{MP2} is the MP2 energy formed from exact ERIs (without the THC or DF approximations) for the mth molecule. The inner sum is equal to the DF-MP2 energy plus the LS-THC-DF-MP2 energy minus twice the MP2 energy formed with mixed integrals. This will be proportional to the MP2 energy for each molecule and therefore we weight each molecule contribution in order to ensure that all molecules in the test set contribute equally to the objective function.[49] The Broyden–Fletcher–Goldfarb–Shanno (BFGS) optimization approach, applying Brent's line search algorithm, is used to optimize the radial nodes.[71−75]

IV. COMPUTATIONAL DETAILS

LS-THC-DF-MP2 has been implemented in a development version of the PSI4 quantum chemistry package.[76] For the LS-THC-DF-MP2 and DF-MP2 calculations, we use Dunning's cc-pVXZ basis with the cc-pVXZ-RI fitting basis set (where X = D,T). In the preceding Hartree–Fock calculations, we use the cc-pVXZ-JKFIT fitting basis set.[49,50,77] All THC calculations reported here use the LS-THC-DF-MP2 approach; other THC variants are possible, as discussed in our previous work.[57,58] The cc-pVTZ basis set has been used with the weighted least-squares THC variant, but this work is the first to present LS-THC-DF-MP2/cc-pVTZ results.[59] All tests for timing purposes are performed using a single core on a quad-core AMD Opteron 2376 processor running at 2.3 GHz.

IV.A. Grid Optimization Training Set. Full details of the molecules used as a training set for the cc-pVDZ and cc-pVTZ grid optimizations are given in Table S1 and Section VII.A of the Supporting Information. The 52 molecules in the THC training set were selected to optimize grid parameters for hydrogen, boron, carbon, nitrogen, oxygen, and fluorine. These molecules range in size from 12 atoms to 42 atoms and include dipeptides, nucleobases, dyes, hydrocarbons, boronated molecules, and fluorinated molecules. The training set geometries were optimized at the B3LYP/6-31G* level.

IV.B. Test Sets. After the grids were optimized using the training sets, we then chose different sets of molecules to test the performance and accuracy of the optimized grids. These test sets include water clusters, alkanes and alkenes, polypeptide conformations, and nucleobase pairs. Geometries for all of the molecules in the test sets either are provided in the Supporting Information (Sections VII.B and VII.C) or are available from previous work.

The performance improvements from the grid optimization are demonstrated with a set of water clusters ranging from $(H_2O)_{10}$ to $(H_2O)_{50}$. Here, we compare the accuracy using LS-THC-DF-MP2 with our previous R-DVR grids and with the optimized grids reported in this article. We also include larger water clusters up to $(H_2O)_{150}$ in order to demonstrate the feasibility of large molecules with LS-THC-DF-MP2. The geometries for these water clusters were obtained by taking snapshots from a molecular dynamics simulation using the TIP3P force field.[57,78]

We test the accuracy of conformational energies using the torsional potential of 1,3,5,7-octatetraene and the set of 27 alanine tetrapeptide conformations reported by DiStasio et al.[79] The E and Z octatetraene geometries were optimized at the MP2/cc-pVDZ level using MOLPRO, version 2010.1.[80] Remaining octatetraene geometries were obtained by linear interpolation in internal coordinates between the optimized E and Z end points. The alanine tetrapeptide conformations follow the same numbering scheme given by DiStasio et al. These geometries were optimized by DiStasio et al. at the HF/6-31G** level of theory.

We demonstrate the practical scaling behavior of LS-THC-DF-MP2 using a set of linear alkanes (from C_4H_{10} through $C_{20}H_{42}$).[58,81] These scaling tests are carried out with both cc-pVDZ and cc-pVTZ basis sets. We also explore the accuracy of the LS-THC-DF-MP2 method in different basis sets using a set of small water cluster geometries previously optimized at the MP2/heavy-aug-cc-pVTZ level by Bates et al.[81]

The accuracy of LS-THC-DF-MP2 for weak interactions is tested using the nucleobase pair test set (JSCH) constructed by Jurečka and co-workers.[82] The JSCH set contains three types of interaction motifs: hydrogen bonding, interstrand, and stacked bases. Geometries in the JSCH set containing sulfur were excluded from this study because we have not yet performed grid optimization for the third-row elements (although this is planned). The JSCH set includes both optimized and experimental geometries.[82] We adopt the geometry reassignments suggested by Burns et al.[83]

Finally, we assess the accuracy of LS-THC-DF-MP2 for barrier heights by using a set of pericyclic reactions. The geometries used here (reactants, products, and transition states) were optimized at the B3LYP/6-31G* level by Guner and co-workers.[84]

V. RESULTS

V.A. Water Clusters. In order to demonstrate the improvements made by the Handy grid optimization procedure, Table 1 compares the LS-THC-DF-MP2 results for a set of water clusters from $(H_2O)_{10}$ to $(H_2O)_{50}$ using the original R-DVR grids, the trimmed R-DVR grid used as an initial guess in the optimization, and the optimized Handy grids. Notice that the LS-THC-DF-MP2 results with the optimized grids use significantly fewer grid points to achieve a similar level of accuracy as that of LS-THC-DF-MP2 results with the R-DVR grids. The compact, optimized Handy grids improve the applicability of LS-THC-DF-MP2 to large chemical systems.

DOI: 10.1021/acs.jctc.5b00272
J. Chem. Theory Comput. 2015, 11, 3042−3052

Table 1. Comparison of LS-THC-DF-MP2/cc-pVDZ with the Original R-DVR Grids to LS-THC-DF-MP2/cc-pVDZ with Handy Grids Built from the Parameters Used To Seed the Grid Optimization Procedure (Trimmed R-DVR) and LS-THC-DF-MP2/cc-pVDZ with the Optimized cc-pVDZ Handy Grids[a]

	original R-DVR		trimmed R-DVR		optimized Handy	
no. water molecules	pts/atom	error (kcal/mol)	pts/atom	error (kcal/mol)	pts/atom	error (kcal/mol)
10	162	0.0004	73	0.0012	73	0.0007
20	162	0.0012	73	0.0111	73	0.0052
30	162	0.0043	73	0.0165	73	0.0096
40	162	0.0038	73	0.0226	73	0.0099
50	162	0.0081	73	0.0394	73	0.0195

[a]Pts/atom denotes the average number of grid points per atom and the errors are given with respect to the DF-MP2/cc-pVDZ results.

Figure 1 shows the absolute error incurred by the THC approximation (compared to DF-MP2) for a set of water

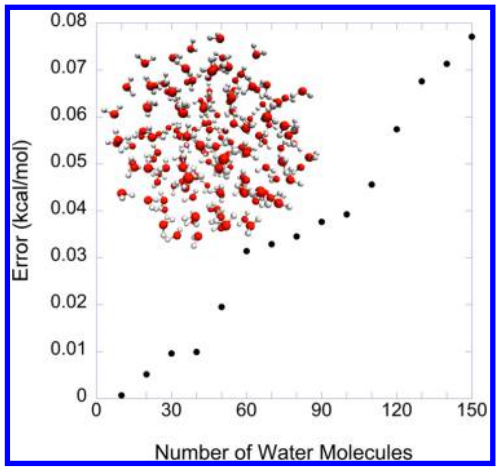

Figure 1. Error in the LS-THC-DF-MP2 energy compared to that of DF-MP2 in kcal/mol. Both calculations used the cc-pVDZ basis and the cc-pVDZ-RI fitting basis.

clusters ranging from $(H_2O)_{10}$ to $(H_2O)_{150}$. As expected from any integral approximation, the error does increase with increasing system size (roughly linearly). This behavior is also observed for the error of DF-MP2 compared to that of canonical MP2 with the exact four-index ERIs. The important point is that the magnitude of the THC error is very small: usually 2 orders of magnitude less than the DF error (which is already widely considered to be acceptable) and always less than 0.1 kcal/mol in the results shown in Figure 1. Thus, the THC approximation is well within the 1 kcal/mol bound often cited as constituting chemical accuracy.

V.B. Conformational Energies. The results for the rotation about the central bond of 1,3,5,7-octatetraene are given in Figure 2. The MP2, DF-MP2, and LS-THC-DF-MP2 results are graphically indistinguishable. Even with the very sparse grids being used, the potential energy curve from LS-THC-DF-MP2 is quite smooth and free of numerical artifacts. Some statistical analysis of both relative and absolute errors is presented in Table 2, where we report separately the error arising from the DF and THC approximations. These data show that the absolute energy error arising from the THC approximation is more than 2 orders of magnitude less than the

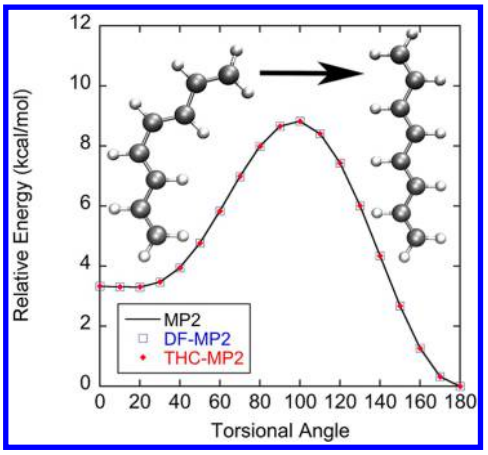

Figure 2. MP2, LS-THC-DF-MP2, and DF-MP2 energies relative to the *E*-geometry (180°) of 1,3,5,7-octatetraene. All calculations were run with the cc-pVDZ basis. The cc-pVDZ-RI fitting basis set was used for both DF-MP2 and LS-THC-DF-MP2 calculations.

Table 2. Unsigned Absolute and Relative Energy Errors (kcal/mol) in LS-THC-DF-MP2 with Respect to MP2/cc-pVDZ (DF+THC), DF-MP2 with Respect to MP2/cc-pVDZ (DF), and LS-THC-DF-MP2 Relative to DF-MP2 (THC) for the Rotation of 1,3,5,7-Octatetraene about the Central Bond[a]

	DF + THC	DF	THC
max unsigned error	0.46106	0.45938	0.00168
average unsigned error	0.45779	0.45741	0.00078
max relative energy error	0.00772	0.00527	0.00245
average relative energy error	0.00469	0.00348	0.00121

[a]Both DF-MP2 and LS-THC-DF-MP2 were calculated with the cc-pVDZ basis and the cc-pVDZ-RI auxiliary basis.

error arising from the DF approximation. The THC contribution to errors in energy differences (denoted relative energy error in Table 2) along this torsional curve is negligible and also smaller than the DF contribution.

The accuracy of LS-THC-DF-MP2 and DF-MP2 energies compared to that of conventional MP2 for 27 different alanine tetrapeptide conformations is shown in Figure 3. The THC approximation introduces less than 0.05 kcal/mol error on top of the roughly 0.1 kcal/mol error introduced by the DF approximation. Both LS-THC-DF-MP2 and DF-MP2 correctly predict the ordering of conformational energies compared to that with the MP2 calculation. Thus, LS-THC-DF-MP2 is quantitatively accurate with respect to DF-MP2 and MP2 for conformational energies of a relatively large system. Further details are included in Sections III and IV of the Supporting Information. Some statistics of the errors introduced by DF and THC are provided in Table 3. We point out that the THC errors in conformational energies are almost an order of magnitude smaller than the corresponding errors in absolute energies, indicating favorable error cancellation for relative properties. We also note that DF-MP2 has already been widely accepted, suggesting that any additional errors introduced by the THC approximation are negligible.

V.C. Basis Sets. The grid optimization scheme was used to optimize separate THC grids for use with the cc-pVDZ and cc-pVTZ basis sets. The number of grid points N_P in the optimized cc-pVDZ grids is approximately 3 times the number of cc-pVDZ-RI basis functions. The optimized cc-pVTZ grids

DOI: 10.1021/acs.jctc.5b00272
J. Chem. Theory Comput. 2015, 11, 3042−3052

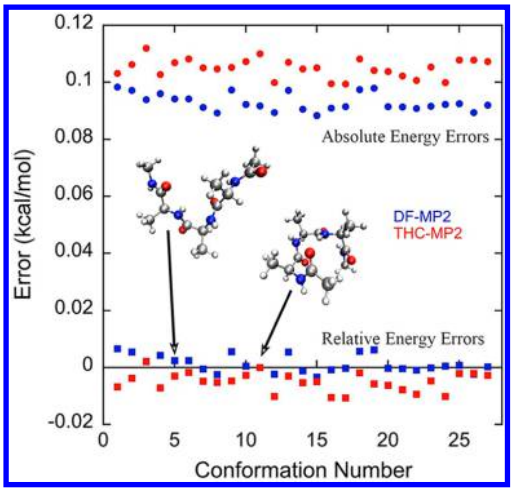

Figure 3. Absolute and relative errors in the DF-MP2 and LS-THC-DF-MP2 alanine tetrapeptide conformational energies (kcal/mol) compared to those with MP2/cc-pVDZ. The zero of the energy is chosen as the global minimum (conformer 11) for the relative energy comparison. Both DF-MP2 and LS-THC-DF-MP2 use the cc-pVDZ basis and the cc-pVDZ-RI auxiliary basis.

Table 3. Unsigned Relative Energy Errors (kcal/mol) of LS-THC-DF-MP2 Compared to MP2/cc-pVDZ (DF+THC), DF-MP2 Compared to MP2/cc-pVDZ (DF), and LS-THC-DF-MP2 Relative to DF (THC) for a Set of Alanine Tetrapeptide Conformations[a]

	DF + THC	DF	THC
max unsigned error	0.11203	0.09830	0.01839
average unsigned error	0.10499	0.09300	0.01199
max relative energy error	0.01061	0.00653	0.01332
average relative energy error	0.00534	0.00243	0.00647

[a]Both DF-MP2 and LS-THC-DF-MP2 use the cc-pVDZ basis and the cc-pVDZ-RI auxiliary basis.

are somewhat larger, with N_P equal to approximately 4 times the number of cc-pVTZ-RI basis functions. We investigate the effect of basis set quality on the observed scaling by using a set of linear alkanes. As shown in Figure 4, the scaling is practically

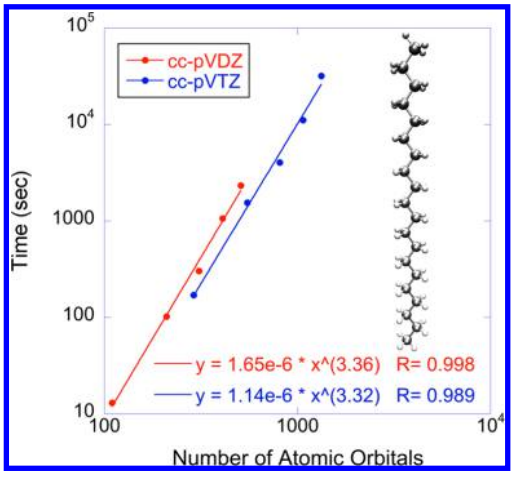

Figure 4. Timings of LS-THC-DF-MP2 calculations for the linear alkanes $CH_3(CH_2)_2CH_3$ to $CH_3(CH_2)_{18}CH_3$ using the cc-pVDZ and cc-pVTZ basis sets. These timings were obtained using one thread on a 2.3 GHz quad-core AMD Opteron processor.

unaffected by the basis set quality. Slight differences in the observed scaling for the cc-pVDZ and cc-pVTZ calculations are in part due to the different sizes of the optimized grids relative to the analogous RI basis sets. Furthermore, the observed scaling is nearly cubic, in spite of the fact that the formal scaling for LS-THC-DF-MP2 is quartic. The origin of this is the dominance of lower-scaling terms and our use of highly efficient matrix multiplication routines for the most computationally involved steps.

In order to test the accuracy of the THC approximation with different basis sets, LS-THC-DF-MP2 and DF-MP2 were applied to a set of water clusters ranging in size from $(H_2O)_3$ to $(H_2O)_{10}$ and using the cc-pVDZ and cc-pVTZ basis sets. Detailed relative energies can be found in Section V of the Supporting Information.

In Figure 5, we compare the energies (relative to the global minimum) from DF-MP2 and LS-THC-DF-MP2 for water

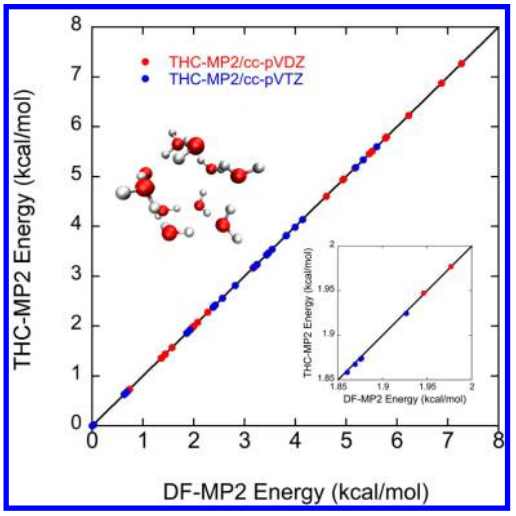

Figure 5. Comparison of DF-MP2 and LS-THC-DF-MP2 for a set of $(H_2O)_{10}$ configurations (representative example shown in the inset) computed with the cc-pVDZ and cc-pVTZ basis sets. All energies are relative to the lowest energy configuration (which is the same in DF-MP2 and LS-THC-DF-MP2). The cc-pVDZ and cc-pVTZ DF-MP2 and LS-THC-DF-MP2 calculations used the cc-pVDZ-RI and cc-pVTZ-RI fitting basis sets, respectively. Lower right inset shows the same data on an expanded scale.

decamers. Excellent agreement is obtained for both cc-pVDZ and cc-pVTZ basis sets. The inset shows an expanded view of the comparison for some of the low-energy structures. Figure 6 shows the maximum absolute energy error from the DF and THC approximations for the whole set of water clusters (from trimers to decamers). Note the different scales used for the DF and THC errors. The DF-MP2 absolute energies are within 0.25 kcal/mol of the MP2 energies for all of the geometries in the set. The further error from the THC approximation is less than 0.0015 kcal/mol in all cases and completely negligible compared to the error induced by the DF approximation. Furthermore, the THC error is only very weakly dependent on the basis set (cc-pVDZ compared to cc-pVTZ). As demonstrated in Figure 1, the THC error does increase with molecular size (and so also does the DF error), but the error is so small that this size-dependence is unimportant.

V.D. Nucleobase Pair Interactions. The JSCH set comprises three main geometry types, representative of the dominant nucleobase pair interactions in DNA duplexes. The

DOI: 10.1021/acs.jctc.5b00272
J. Chem. Theory Comput. 2015, 11, 3042−3052

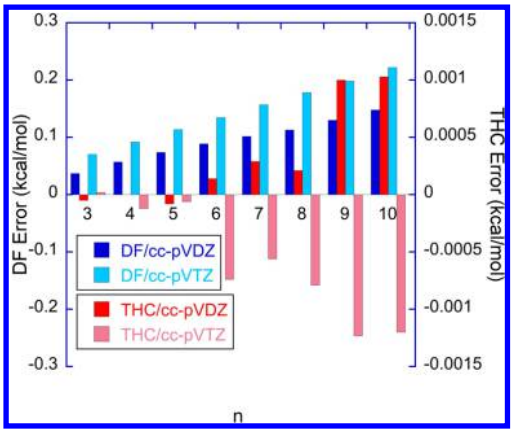

Figure 6. For the set of water clusters $(H_2O)_n$ with n = 3−10, the maximum absolute errors (kcal/mol) of LS-THC-DF-MP2 with respect to MP2 were determined. These total errors are broken into the error components of DF-MP2 with respect to MP2 (DF) and LS-THC-DF-MP2 relative to DF-MP2 (THC). Notice that the scales for the DF and THC errors differ by 2 orders of magnitude. The cc-pVDZ and cc-pVTZ basis sets were used with the cc-pVDZ-RI and cc-pVTZ-RI fitting basis sets, respectively, for the DF-MP2 and LS-THC-DF-MP2 calculations. The MP2 reference calculations use the cc-pVDZ and cc-pVTZ basis sets.

hydrogen-bonded geometries consist of coplanar nucleobase pairs, whereas the interstrand geometries involve adjacent base pairs on different strands. The stacked complex type is composed of adjacent base pairs on the same strand. The interaction energies reported include the counterpoise correction. All interaction energies can be found in Section VI of the Supporting Information. Figure 7 shows the percentage error in the interaction energies computed by LS-THC-DF-MP2 compared to the DF-MP2 interaction energies. The average percentage error for the three different classes is

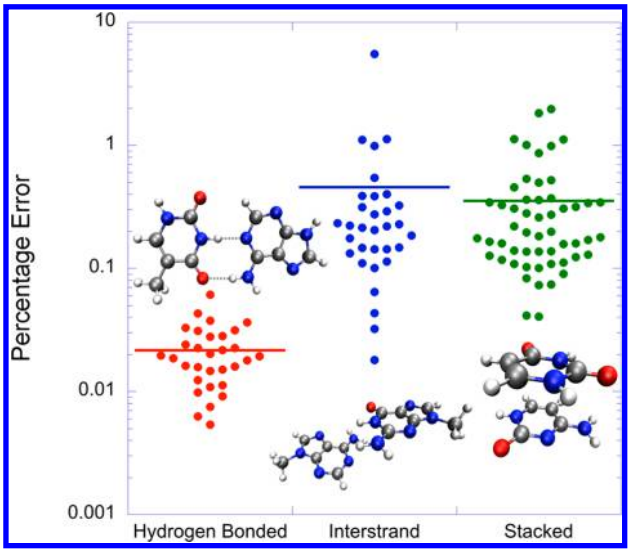

Figure 7. Percentage error in LS-THC-DF-MP2/cc-pVDZ counterpoise-corrected interaction energies of nucleobase pairs (from the JSCH database) relative to DF-MP2/cc-pVDZ counterpoise-corrected interaction energies. The cc-pVDZ-RI fitting basis was used for the DF-MP2 and LS-THC-DF-MP2 calculations. Results are separated into three classes of geometric configurations, and the solid bar represents the average percentage error within each of these subgroups.

denoted with a solid line and is less than 1% for all three cases. Many of the interaction energies being computed in this test set are quite small (<1 kcal/mol), and one should bear this in mind when assessing the percentage error. Indeed, the largest absolute error arising from the THC approximation for an interaction energy in this test set is less than 0.05 kcal/mol.

V.E. Reaction Barrier Heights. To probe the accuracy of the THC approximation for computing barrier heights, a subset of reactions was taken from a pericyclic reaction database.[84] These reactions are summarized in Figure 8, along with the

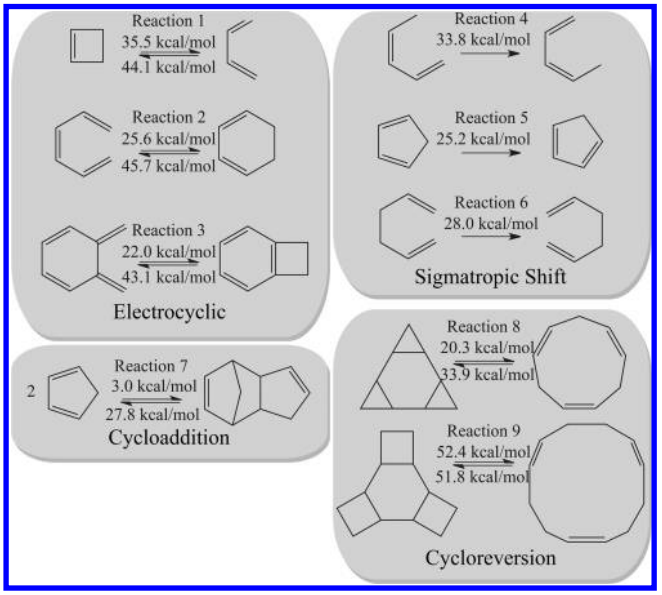

Figure 8. Set of pericyclic reactions used to calculate barrier heights. The approximate barrier heights are computed at the MP2/cc-pVDZ level.

estimated reaction barrier heights computed with canonical MP2 and the cc-pVDZ basis set. The estimated reaction barrier heights in this work refer to the difference in the transition state and reactant energies without zero-point corrections. The geometries for the reactants and transition states are taken from previous work without reoptimization.

Figure 9 compares the unsigned errors in the computed barrier heights using LS-THC-DF-MP2 and DF-MP2 relative to that with canonical MP2. As can be seen, the error introduced by the THC approximation is very small and less than the error introduced by the widely used DF approximation. The ring opening of cyclobutene (reaction 6) has the highest total unsigned error compared to that of the other reactions, but even this is well within chemical accuracy (<0.3 kcal/mol). Curiously, both DF-MP2 and LS-THC-DF-MP2 underestimate all of the pericyclic reaction barrier heights. Quantitative statistics for the errors are given in Table 5. For all of the reaction barrier height estimations, LS-THC-DF-MP2 and DF-MP2 are in good agreement with the canonical MP2 results. Furthermore, the error introduced by the THC approximation is an order of magnitude less than the error introduced by the DF approximation.

VI. CONCLUSIONS

DF-MP2 benefits markedly from the use of optimized auxiliary basis sets, so it is not surprising that the LS-THC-DF-MP2 method similarly benefits from an optimized grid. To avoid the

DOI: 10.1021/acs.jctc.5b00272
J. Chem. Theory Comput. 2015, 11, 3042−3052

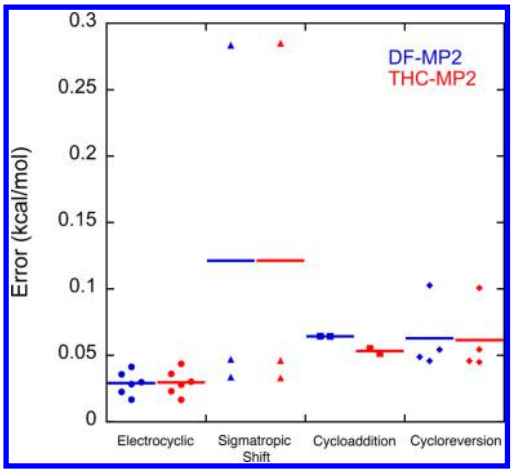

Figure 9. Absolute errors in the estimated barrier heights relative to the MP2/cc-pVDZ estimated barrier heights for the pericyclic reactions found in Figure 8. The results are split into pericyclic reaction types, with solid bars used to indicate the average estimated barrier height errors for DF-MP2 and LS-THC-DF-MP2. All calculations used the cc-pVDZ basis set. Both DF-MP2 and LS-THC-DF-MP2 were calculated with the cc-pVDZ basis and the cc-pVDZ-RI auxiliary basis.

Table 5. LS-THC-DF-MP2 Errors (kcal/mol) in Barrier Heights with Respect to the Barrier Heights Calculated at the MP2/cc-pVDZ Level (Total), DF-MP2 Errors with Respect to MP2 (DF), and LS-THC-DF-MP2 Error Relative to DF-MP2 (THC) for the Reactions Found in Figure 8[a]

	total	DF	THC
max unsigned error	0.2849	0.2835	0.0130
average unsigned error	0.0596	0.0612	0.0023

[a]Both DF-MP2 and LS-THC-DF-MP2 were calculated with the cc-pVDZ basis and the cc-pVDZ-RI auxiliary basis.

issue of unnecessarily dense grids, this work outlined a procedure to optimize the locations of radial nodes in order to form compact grids that achieve a high level of accuracy. The level of accuracy achieved using these grids indicates that optimizing the radial nodes for each element results in a more compact grid representation of the relevant physical space surrounding that element within the molecular environment. This procedure also allows the extension of THC to larger basis sets, and we demonstrated this for triple-ζ cc-pVTZ basis sets.

The LS-THC approach has no system-specific approximations and should be applicable, therefore, to any system of interest. For example, it is not affected by electronic delocalization that can cause difficulties in local approximations. We applied LS-THC-DF-MP2 to test sets emphasizing conformational energetics, interaction energies, and reaction barrier heights. In all cases, the LS-THC-DF-MP2 results were well within chemical accuracy. Energy differences, such as conformational energies and reaction barrier heights, benefit from a favorable cancellation of errors. This is in contrast to many numerical grid-based approaches where the associated errors are often quite random.

This work is also the first to investigate the LS-THC approximation with increasing basis set quality. Similar to the DF approximation, LS-THC exploits rank sparsity in the ERIs. In DF methods, the size of the auxiliary fitting basis set needed for a given accuracy increases slowly relative to the basis set density. This is because the rank of the ERIs does not increase much as the basis set density increases. We believe that this should also be true for the auxiliary grids used in LS-THC, and the comparison of the grids for double-ζ and triple-ζ basis sets in this article supports that. This is cause for optimism regarding the ability of THC to efficiently accommodate larger basis sets including diffuse functions. Work is in progress to demonstrate this and also to adapt the outlined procedure to optimize THC grids for coupled cluster methods, where the THC approximation has already been employed effectively.[59−62]

■ ASSOCIATED CONTENT

Supporting Information

Further details regarding the computation of the Handy radial weights and the THC grid optimization procedure. Optimized THC grid parameters for the cc-pVDZ and cc-pVTZ basis sets. Additional information regarding the errors in the octatetraene, alanine conformation, water cluster, and nucleobase pair interaction computations. Geometry information for the THC grid optimization training set, the water cluster $(H_2O)_{10}$−$(H_2O)_{150}$ set, and the octatetraene set. The Supporting Information is available free of charge on the ACS Publications website at DOI: 10.1021/acs.jctc.5b00272.

■ AUTHOR INFORMATION

Corresponding Author

*E-mail: todd.martinez@stanford.edu.

Funding

This work was supported by the National Science Foundation (OCI-1047577) and by the Department of Defense (Office of the Assistant Secretary of Defense for Research and Engineering) through a National Security Science and Engineering Faculty Fellowship to T.J.M. S.I.L.K.S. is grateful for support from the National Science Foundation through a Blue Waters Graduate Fellowship. This research is part of the Blue Waters sustained-petascale computing project, which is supported by the National Science Foundation (awards OCI-0725070 and ACI-1238993) and the state of Illinois. Blue Waters is a joint effort of the University of Illinois at Urbana−Champaign and its National Center for Supercomputing Applications. R.M.P. is supported by a DOE Computational Science Graduate Fellowship (grant no. DE-FG02-97ER25308).

Notes

The authors declare no competing financial interest.

■ REFERENCES

(1) Møller, C.; Plesset, M. S. Note on an approximation treatment for many-electron systems. *Phys. Rev.* **1934**, *46*, 618.

(2) Ayala, P. Y.; Scuseria, G. E. Linear scaling second-order Møller−Plesset theory in the atomic orbital basis for large molecular systems. *J. Chem. Phys.* **1999**, *110*, 3660.

(3) Ayala, P. Y.; Kudin, K. N.; Scuseria, G. E. Atomic orbital Laplace-transformed second-order Møller−Plesset theory for periodic systems. *J. Chem. Phys.* **2001**, *115*, 9698.

(4) Pulay, P.; Saebø, S.; Wolinski, K. Efficient calculation of canonical MP2 energies. *Chem. Phys. Lett.* **2001**, *344*, 543.

(5) Lambrecht, D. S.; Doser, B.; Ochsenfeld, C. Rigorous integral screening for electron correlation methods. *J. Chem. Phys.* **2005**, *123*, 184102.

(6) Doser, B.; Lambrecht, D. S.; Kussmann, J.; Ochsenfeld, C. Linear-scaling atomic orbital-based second-order Møller−Plesset perturbation theory by rigorous integral screening criteria. *J. Chem. Phys.* **2009**, *130*, 064107.

DOI: 10.1021/acs.jctc.5b00272
J. Chem. Theory Comput. 2015, 11, 3042−3052

(7) Vahtras, O.; Almlöf, J.; Feyereisen, M. W. Integral approximations for LCAO-SCF calculations. *Chem. Phys. Lett.* **1993**, *213*, 514.
(8) Doser, B.; Lambrecht, D. S.; Ochsenfeld, C. Tighter multipole-based integral estimates and parallel implementation of linear-scaling AO-MP2 theory. *Phys. Chem. Chem. Phys.* **2008**, *10*, 3335.
(9) Pulay, P. Localizability of dynamic electron correlation. *Chem. Phys. Lett.* **1983**, *100*, 151.
(10) Pulay, P.; Saebø, S. Orbital-invariant formulation and second-order gradient evaluation in Møller−Plesset perturbation theory. *Theor. Chim. Acta* **1986**, *69*, 357.
(11) Saebø, S.; Pulay, P. Local treatment of electron correlation. *Annu. Rev. Phys. Chem.* **1993**, *44*, 213.
(12) Friesner, R. A.; Murphy, R. B.; Beachy, M. D.; Ringnalda, M. N.; Pollard, W. T.; Dunietz, B. D.; Cao, Y. Correlated ab initio electronic structure calculations for large molecules. *J. Phys. Chem. A* **1999**, *103*, 1913.
(13) Lee, M. S.; Maslen, P. E.; Head-Gordon, M. Closely approximating second-order Møller−Plesset perturbation theory with a local triatomics in molecules model. *J. Chem. Phys.* **2000**, *112*, 3592.
(14) Meyer, W. Ionization energies of water from PNO-CI calculations. *Int. J. Quantum Chem.* **1971**, *5*, 341.
(15) Meyer, W. PNO-CI Studies of electron correlation effects. I. Configuration expansion by means of nonorthogonal orbitals and application to the ground and ionized states of methane. *J. Chem. Phys.* **1973**, *58*, 1017.
(16) Neese, F.; Hansen, A.; Liakos, D. G. Efficient and accurate approximations to the local coupled cluster singles doubles method using a truncated pair natural orbital basis. *J. Chem. Phys.* **2009**, *131*, 064103.
(17) Neese, F.; Wenmohs, F.; Hansen, A. Efficient and accurate local approximations to coupled electron-pair approaches: An attempt to revive the pair natural orbital method. *J. Chem. Phys.* **2009**, *130*, 114108.
(18) Yang, J.; Kurashige, Y.; Manby, F. R.; Chan, G. K. L. Tensor factorizations of local second-order Møller−Plesset theory. *J. Chem. Phys.* **2011**, *134*, 044123.
(19) Yang, J.; Chan, G. K. L.; Manby, F. R.; Schuetz, M.; Werner, H. J. The orbital-specific-virtual local coupled cluster singles and doubles method. *J. Chem. Phys.* **2012**, *136*, 144105.
(20) Kurashige, Y.; Yang, J.; Chan, G. K. L.; Manby, F. R. Optimization of orbital-specific virtuals in local Møller−Plesset perturbation theory. *J. Chem. Phys.* **2012**, *136*, 124106.
(21) Riplinger, C.; Neese, F. An efficient and near linear scaling pair natural orbital based local coupled cluster method. *J. Chem. Phys.* **2013**, *138*, 034106.
(22) Schütz, M.; Hetzer, G.; Werner, H.-J. Low-order scaling local electron correlation methods. I. Linear scaling local MP2. *J. Chem. Phys.* **1999**, *111*, 5691.
(23) Werner, H.-J.; Manby, F. R.; Knowles, P. J. Fast linear scaling second-order Møller−Plesset perturbation theory (MP2) using local and density fitting approximations. *J. Chem. Phys.* **2003**, *118*, 8149.
(24) Maurer, S. A.; Lambrecht, D. S.; Kussmann, J.; Ochsenfeld, C. Efficient distance-including integral screening in linear-scaling Møller−Plesset perturbation theory. *J. Chem. Phys.* **2013**, *138*, 014101.
(25) Kussmann, J.; Beer, M.; Ochsenfeld, C. Linear scaling self-consistent field methods for large molecules. *Wiley Interdiscip. Rev.: Comput. Mol. Sci.* **2013**, *3*, 614.
(26) Saebo, S. Linear scaling second order Møller−Plesset theory. In *Linear Scaling Techniques in Computational Chemistry and Physics: Methods and Applications*; Zalesny, R., Papadopoulos, M. G., Mezey, P. G., Leszczynski, J., Eds.; Springer: Dordrecht, The Netherlands, 2011; Vol. *13*, p 65.
(27) Subotnik, J. E.; Sodt, A.; Head-Gordon, M. The limits of local correlation theory: electronic delocalization and chemically smooth potential energy surfaces. *J. Chem. Phys.* **2008**, *128*, 034103.
(28) Russ, N. J.; Crawford, T. D. Potential energy surface discontinuities in local correlation methods. *J. Chem. Phys.* **2004**, *121*, 691.
(29) Friesner, R. A. Solution of self-consistent field electronic structure equations by a pseudospectral method. *Chem. Phys. Lett.* **1985**, *116*, 39.
(30) Friesner, R. A. Solution of the Hartree−Fock equations by a pseudospectral method: application to diatomic molecules. *J. Chem. Phys.* **1986**, *85*, 1462.
(31) Friesner, R. A. Solution of the Hartree−Fock equations for polyatomic molecules by a pseudospectral method. *J. Chem. Phys.* **1987**, *86*, 3522.
(32) Friesner, R. A. New methods for electronic structure calculations on large molecules. *Annu. Rev. Phys. Chem.* **1991**, *32*, 341.
(33) Martínez, T. J.; Carter, E. A. Pseudospectral Møller−Plesset perturbation theory through third order. *J. Chem. Phys.* **1994**, *100*, 3631.
(34) Martínez, T. J.; Carter, E. A. Pseudospectral methods applied to the electron correlation problem. In *Modern Electronic Structure Theory*; Yarkony, D. R., Ed.; World Scientific: Singapore, 1995; Vol. *2*, p 1132.
(35) Beebe, N. H. F.; Linderberg, J. Simplifications in the generation and transformation of two-electron integrals in molecular calculations. *Int. J. Quantum Chem.* **1977**, *12*, 683.
(36) Røeggen, I.; Wisløff-Nilssen, E. On the Beebe−Linderberg two-electron integral approximation. *Chem. Phys. Lett.* **1986**, *132*, 154.
(37) Koch, H.; de Merás, A. S.; Pedersen, T. B. Reduced scaling in electronic structure calculations using Cholesky decompositions. *J. Chem. Phys.* **2003**, *118*, 9481.
(38) Weigend, F.; Kattannek, M.; Ahlrichs, R. Approximated electron repulsion integrals: Cholesky decomposition versus resolution of the identity methods. *J. Chem. Phys.* **2009**, *130*, 164106.
(39) Dunlap, B. I.; Connolly, J. W. D.; Sabin, J. R. On the applicability of LCAO-Xα methods to molecules containing transition metal atoms: the nickel atom and nickel hydride. *Int. J. Quantum Chem.* **1977**, *S11*, 81.
(40) Dunlap, B. I.; Connolly, J. W. D.; Sabin, J. R. On some approximations in applications of Xα theory. *J. Chem. Phys.* **1979**, *71*, 3396.
(41) Feyereisen, M.; Fitzgerald, G.; Komornicki, A. Use of approximate integrals in ab initio theory. An application in MP2 energy calculations. *Chem. Phys. Lett.* **1993**, *208*, 359.
(42) Bernholdt, D. E.; Harrison, R. J. Large-scale correlated electronic structure calculations: the RI-MP2 method on parallel computers. *Chem. Phys. Lett.* **1996**, *250*, 477.
(43) Kendall, R. A.; Früchtl, H. A. The impact of the resolution of the identity approximate integral method on modern ab initio algorithm development. *Theor. Chem. Acc.* **1997**, *97*, 158.
(44) Bernholdt, D. E.; Harrison, R. J. Fitting basis sets for the RI-MP2 approximate second-order many-body perturbation theory method. *J. Chem. Phys.* **1998**, *109*, 1593.
(45) Baerends, E. J.; Ellis, D. E.; Ros, P. Self-consistent molecular Hartree−Fock−Slater calculations I. The computational procedure. *Chem. Phys.* **1973**, *2*, 41.
(46) Whitten, J. L. Coulombic potential energy integrals and approximations. *J. Chem. Phys.* **1973**, *58*, 4496.
(47) Almlöf, J. Elimination of energy denominators in Møller−Plesset perturbation theory by a Laplace transform approach. *Chem. Phys. Lett.* **1991**, *181*, 319.
(48) Jung, Y.; Sodt, A.; Gill, P. M. W.; Head-Gordon, M. Auxiliary basis expansions for large-scale electronic structure calculations. *Proc. Natl. Acad. Sci. U.S.A.* **2005**, *102*, 6692.
(49) Weigend, F.; Häser, M.; Patzelt, H.; Ahlrichs, R. RI-MP2: optimized auxiliary basis sets and demonstration of efficiency. *Chem. Phys. Lett.* **1998**, *294*, 143.
(50) Weigend, F.; Köhn, A.; Hättig, C. Efficient use of the correlation consistent basis sets in resolution of the identity MP2 calculations. *J. Chem. Phys.* **2002**, *116*, 3175.
(51) Benedikt, U.; Auer, A. A.; Espig, M.; Hackbusch, W. Tensor decomposition in post-Hartree−Fock methods. I. Two-electron integrals and MP2. *J. Chem. Phys.* **2011**, *134*, 054118.

DOI: 10.1021/acs.jctc.5b00272
J. Chem. Theory Comput. 2015, 11, 3042−3052

(52) Benedikt, U.; Bohm, K.-H.; Auer, A. A. Tensor decomposition in post-Hartree−Fock methods. II. CCD implementation. *J. Chem. Phys.* **2013**, *139*, 224101.
(53) Feller, D.; Aprà, E.; Nichols, J. A.; Bernholdt, D. E. The structure and binding energy of K^+−ether complexes: a comparison of MP2, RIMP2, and density functional methods. *J. Chem. Phys.* **1996**, *105*, 1940.
(54) Weigend, F.; Häser, M. RI-MP2: first derivatives and global consistency. *Theor. Chem. Acc.* **1997**, *97*, 331.
(55) Bostrom, J.; Aquilante, F.; Pedersen, T. B.; Lindh, R. Ab initio density fitting: accuracy assessment of auxiliary basis sets from Cholesky decompositions. *J. Chem. Theor. Comp.* **2009**, *5*, 1545.
(56) Weigend, F. A fully direct RI-HF algorithm: implementation, optimized auxiliary basis sets, demonstration of accuracy and efficiency. *Phys. Chem. Chem. Phys.* **2002**, *4*, 4285.
(57) Hohenstein, E. G.; Parrish, R. M.; Martínez, T. J. Tensor hypercontraction density fitting. I. Quartic scaling second- and third-order Møller−Plesset perturbation theory. *J. Chem. Phys.* **2012**, *137*, 044103.
(58) Parrish, R. M.; Hohenstein, E. G.; Martínez, T. J.; Sherrill, C. D. Tensor hypercontraction. II. Least-squares renormalization. *J. Chem. Phys.* **2012**, *137*, 224106.
(59) Parrish, R. M.; Sherrill, C. D.; Hohenstein, E. G.; Kokkila, S. I. L.; Martínez, T. J. Accleration of coupled cluster singles and doubles via orbital-weighted least-squares tensor hypercontraction. *J. Chem. Phys.* **2014**, *140*, 181102.
(60) Hohenstein, E. G.; Parrish, R. M.; Sherrill, C. D.; Martínez, T. J. Tensor hypercontraction. III. Least-squares tensor hypercontraction for the determination of correlated wavefunctions. *J. Chem. Phys.* **2012**, *137*, 221101.
(61) Hohenstein, E. G.; Kokkila, S. I. L.; Parrish, R. M.; Martínez, T. J. Tensor hypercontraction equation of motion second-order approximate coupled cluster: electronic excitation energies in $O(N^4)$ time. *J. Phys. Chem. B* **2013**, *117*, 12972.
(62) Hohenstein, E. G.; Kokkila, S. I. L.; Parrish, R. M.; Martínez, T. J. Quartic scaling second-order approximate coupled cluster singles and doubles via tensor hypercontraction: THC-CC2. *J. Chem. Phys.* **2013**, *138*, 124111.
(63) Häser, M.; Almlöf, J. Laplace transform techniques in Møller−Plesset perturbation theory. *J. Chem. Phys.* **1992**, *96*, 489.
(64) Parrish, R. M.; Hohenstein, E. G.; Martínez, T. J.; Sherrill, C. D. Discrete variable representation in electronic structure theory: quadrature grids for least-squares tensor hypercontraction. *J. Chem. Phys.* **2013**, *138*, 194107.
(65) Lebedev, V. I.; Laikov, D. N. A quadrature formula for the sphere of the 131st algebraic order of accuracy. *Dokl. Math.* **1999**, *59*, 477.
(66) Treutler, O.; Ahlrichs, R. Efficient molecular numerical integration schemes. *J. Chem. Phys.* **1995**, *102*, 346.
(67) Murray, C. W.; Handy, N. C.; Laming, G. J. Quadrature schemes for integrals of density functional theory. *Mol. Phys.* **1993**, *78*, 997.
(68) Gill, P. M. W.; Chien, S.-H. Radial quadrature for multi-exponential integrands. *J. Comput. Chem.* **2003**, *24*, 732.
(69) Gill, P. M. W.; Johnson, B. G.; Pople, J. A. A standard grid for density functional calculations. *Chem. Phys. Lett.* **1993**, *209*, 506.
(70) Johnson, B. G.; Gill, P. M. W.; Pople, J. A. A rotationally invariant procedure for density functional calculations. *Chem. Phys. Lett.* **1994**, *220*, 377.
(71) Broyden, C. G. The convergence of a class of double-rank minimization algorithms 1. General considerations. *IMA J. Appl. Math.* **1970**, *6*, 76.
(72) Fletcher, R. A new approach to variable metric algorithms. *Comput. J.* **1970**, *13*, 317.
(73) Goldfarb, D. A family of variable-metric methods derived by variational means. *Math. Comput.* **1970**, *24*, 23.
(74) Shanno, D. F. Conditioning of quasi-Newton methods for function minimization. *Math. Comput.* **1970**, *24*, 647.
(75) Brent, R. P. *Algorithms for Minimization without Derivatives*; Prentice-Hall: Englewood Cliffs, NJ, 1973.
(76) Turney, J. M.; Simmonett, A. C.; Parrish, R. M.; Hohenstein, E. G.; Evangelista, F. A.; Fermann, J. T.; Mintz, B. J.; Burns, L. A.; Wilke, J. J.; Abrams, M. L.; Russ, N. J.; Leininger, M. L.; Janssen, C. L.; Seidl, E. T.; Allen, W. D.; Schaefer, H. F.; King, R. A.; Valeev, E. F.; Sherrill, C. D.; Crawford, T. D. Psi4: an open-source ab initio electronic structure program. *Wiley Interdiscip. Rev.: Comput. Mol. Sci.* **2012**, *2*, 556.
(77) Dunning, T. H., Jr. Gaussian basis sets for use in correlated molecular calculations. I. The atoms boron through neon and hydrogen. *J. Chem. Phys.* **1989**, *90*, 1007.
(78) Case, D. A.; Darden, T. A.; Cheatham , T. E., III; Simmerling, C. L.; Wang, J.; Duke, R. E.; Luo, R.; Walker, R. C.; Zhang, W.; Merz, K. M.; Roberts, B.; Hayik, S.; Roitberg, A.; Seabra, G.; Swails, J.; Götz, A. W.; Kolossváry, I.; Wong, K. F.; Paesani, F.; Vanicek, J.; Wolf, R. M.; Liu, J.; Wu, X.; Brozell, S. R.; Steinbrecher, T.; Gohlke, H.; Cai, Q.; Ye, X.; Wang, J.; Hsieh, M.-J.; Cui, G.; Roe, D. R.; Mathews, D. H.; Seetin, M. G.; Salomon-Ferrer, R.; Sagui, C.; Babin, V.; Luchko, T.; Gusarov, S.; Kovalenko, A.; Kollman, P. A. *AMBER 12*; University of California: San Francisco, CA, 2012.
(79) DiStasio, R. A., Jr.; Jung, Y.; Head-Gordon, M. A resolution-of-the-identity implementation of the local triatomics-in-molecules model for second-order Møller−Plesset perturbation theory with applications to alanine tetrapeptide conformational energies. *J. Chem. Theory Comput.* **2005**, *1*, 862.
(80) Werner, H.-J.; Knowles, P. J.; Knizia, G.; Manby, F. R.; Schütz, M.; et al. *MOLPRO*, 2010.1. http://www.molpro.net.
(81) Bates, D. M.; Smith, J. R.; Tschumper, G. S. Efficient and accurate methods for the geometry optimization of water clusters: application of analytic gradients for the two-body:many-body QM:QM fragmentation method to $(H_2O)_n$, n = 3−10. *J. Chem. Theory Comput.* **2011**, *7*, 2753.
(82) Jurečka, P.; Šponer, J.; Černý, J.; Hobza, P. Benchmark database of accurate (MP2 and CCSD(T) complete basis set limit) interaction energies of small model complexes, DNA base pairs, and amino acid pairs. *Phys. Chem. Chem. Phys.* **2006**, *8*, 1985.
(83) Burns, L. A.; Vázquez-Mayagoitia, Á.; Sumpter, B. G.; Sherrill, C. D. Density-functional approaches to noncovalent interactions: a comparison of dispersion corrections (DFT-D), exchange-hole dipole moment (XDM) theory, and specialized functionals. *J. Chem. Phys.* **2011**, *134*, 084107.
(84) Guner, V.; Khuong, K. S.; Leach, A. G.; Lee, P. S.; Bartberger, M. D.; Houk, K. N. A standard set of pericyclic reactions of hydrocarbons for the benchmarking of computational methods: the performance of an initio, density functional, CASSCF, CASPT2, and CBS-QB3 methods for the prediction of activation barriers, reaction energetics, and transition state geometries. *J. Phys. Chem. A* **2003**, *107*, 11445.

DOI: 10.1021/acs.jctc.5b00272
J. Chem. Theory Comput. 2015, 11, 3042−3052